ACS APPLIED MATERIALS & INTERFACES

Research Article

www.acsami.org

Deterministic Reshaping of Breath Figure Arrays by Directional Photomanipulation

Wei Wang,[†] Yuan Yao,[†] Tianchan Luo,[‡] Lingzhi Chen,[†] Jiaping Lin,*[,†] Lei Li,*[,‡] and Shaoliang Lin*[,†]

[†]Shanghai Key Laboratory of Advanced Polymeric Materials, Key Laboratory for Ultrafine Materials of Ministry of Education, School of Materials Science and Engineering, East China University of Science and Technology, Shanghai 200237, China

[‡]College of Materials, Xiamen University, Xiamen 621005, China

Supporting Information

ABSTRACT: The fabrication of desired structures is one of the most urgent topics in current research on porous polymer films. Herein, directional photomanipulation in conjunction with breath figure processing has been demonstrated for the preparation of porous polymeric films with finely tunable pore shape and size. Because of the photoinduced directional mass migration of azobenzene units upon vertical incident linearly polarized light (LPL) irradiation, round pores on honeycomb films can be reshaped into multifarious shapes including rectangle, rhombus, dumbbell, line, and so forth. In addition, slantwise LPL irradiation produces unique asymmetrical structure inside the pores oriented along the polarized direction. On the other hand, circularly polarized light (CPL) irradiation affords manipulation of the wall thickness without changing the pore shape. This versatile directional photomanipulation method can be implemented to large-area and high-throughput reshaping processes, which paves the way to a number of promising applications such as a flexible etching mask for patterning.

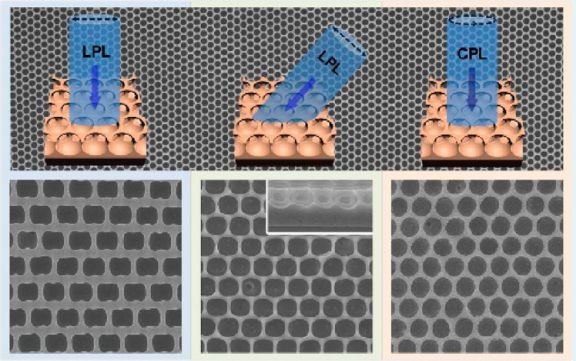

KEYWORDS: *self-assembly, porous films, block copolymers, azobenzene, photomanipulation*

INTRODUCTION

High-throughput and large-scale manufacturable porous polymer films are critical for separation, tissue-engineering, photonic band gap, microelectronics, and lithography.[1−6] Self-assembly is an extremely powerful and effective strategy to fabricate polymer films with various micro/nano morphologies and particular functionality[7−11] in which breath figure (BF) has been adopted as an extraordinary approach to prepare ordered honeycomb-structured porous polymer films because of its low cost, time savings, and easy implementation.[12−14] After casting the polymer solution of water-immiscible solvent under high humidity, the water droplets become nucleated on the solution surface due to the temperature decrease caused by the rapid evaporation of solvent. The condensed microdroplets are subsequently stabilized by the instant precipitation of the polymer enveloping around them and continuously aggregate into a hexagonal array driven by Marangoni convection. The water droplets maintain inherent sphericity because of their high surface tension during the BF process. Eventually, after the solvent and water evaporate completely, isotropic and hexagonally arranged round pores are left on the polymer film surface in most cases, which are called breath figure arrays (BFAs).[15−18]

In recent years, several strategies have been developed to transform the intrinsic round pore and hexagonal close packing of BFAs into diverse shapes and architectures for various applications.[19−22] In a dynamic BF process, definite carrier gas is blown above the polymer solution, exerting forces on water droplets along the flow direction to modify the shape of water droplets from spherical to elliptical with the long axis parallel to the gas flow direction, subsequently forming elliptical pores.[23] Additionally, a variety of physical secondary processing methods, including mechanical stretching or shrinking, are also employed to obtain novel micro/nanostructured BFAs with square-, rectangular-, or triangular-shaped pores.[24−26] However, these methods may incur uncertainties and diminish reproducibility or lead to laceration unless the viscoelasticity of the polymers adapt the distortion stress during the physical processing.

Very recently, we developed a directional photomanipulation technique to tune the surface features of BFAs.[27] This technique was inspired by photofluidization based on the Weigert effect.[28−31] Azobenzene units selectively absorb the linearly polarized light (LPL) whose polarization is direction parallel to their transition moments. Combining the polarization-selective *trans*-to-*cis* isomerization and unselective *cis*-to-*trans* reverse isomerization, the azobenzene units in the *trans* state reorient to a plane orthogonal to the polarization direction

Received: November 2, 2016
Accepted: January 10, 2017
Published: January 10, 2017

DOI: 10.1021/acsami.6b14024
ACS Appl. Mater. Interfaces 2017, 9, 4223−4230

and give rise to mass migration.[32−34] In our previous work, the original round pores on azobenzene-containing block copolymer BF films were converted into rectangular-, rhombic-, and parallelogram-shaped structures within 30 min depending on the polarization direction of the incident light with respect to the orientation of the BFAs. However, the study of photoinduced reconfiguration of BFAs is limited to the operation under vertical incident LPL irradiation on BFAs with identical pristine morphology. It remains a challenge to achieve the detailed investigation of photomanipulation of BFAs for potential applications.

In this work, we present a comprehensive description of the photomanipulation on large area poly(4-vinylpyridine)-*block*-poly[6-[4-(4-butyloxyphenylazo)phenoxy]hexyl methacrylate] (P4VP-*b*-PAzoMA) BFAs by tuning the pristine morphology of the films, constitution of azobenzene-containing polymer, and style and direction of the polarized light. Pores with novel shapes could be deterministically generated upon vertical LPL radiation for certain periods of time depending on the pristine morphology of films and composition of azobenzene polymers. Thanks to the improved static BF process and nondestructive photomanipulation method, large-scale ordered transformed BFAs in a square millimeter have been prepared. Additionally, pores with three-dimensional asymmetrical morphology or controllable wall thickness were also obtained simply through oblique incidence LPL or circularly polarized light (CPL) irradiation. Such a deterministic BFA reshaping strategy is promising for a number of applications such as etching masks.

EXPERIMENTAL SECTION

Materials. The chemical structures of azobenzene-containing polymers are illustrated in Tables S1 and S2. The diblock copolymers P4VP-*b*-PAzoMA with different fractions of two blocks were synthesized via a two-step reversible addition−fragmentation chain transfer polymerization as previously reported.[27] Triblock copolymer poly(ethylene oxide) monomethyl ether-*block*-polystyrene-*block*-{poly[6-(4-methoxy-azobenzene-4′-oxy)hexyl methacrylate]}$_2$ [PEO-*b*-PS-*b*-(PMMAzo)$_2$] was synthesized by a two-step atom transfer radical polymerization (ATRP) as described elsewhere.[29] Diblock copolymer polydimethylsiloxane-*block*-poly[11-[4-(4-butylphenylazo)phenoxy]-undecyl methacrylate)] (PDMS-*b*-PAzoMA) with molecular weight of 2.40×10^4 g mol^{-1} was purchased from Polymer Source, Inc., Canada. Homopolymer PMMAzo was prepared by atom transfer radical polymerization (ATRP) using CuBr/PMDETA as a catalyst system and EtBriB as the initiator as previously reported.[35,36] Poly(styrene-*co*-allyl alcohol) with molecular weight of 2.2×10^3 g mol^{-1} was purchased from Sigma-Aldrich. Water used in all of the experiments was deionized and ultrafiltrated. Other reagents (A.R. grade) were purchased from Adamas-beta and used as received.

Preparation and Photomanipulation of Honeycomb Films. Polymer solutions at different concentrations were prepared by dissolving polymer into carbon disulfide. Glass slides with a size of 0.8 cm^2 were cleaned by ethyl alcohol and subsequently dried in a 50 °C vacuum before use. Honeycomb films were fabricated in a constant temperature and humidity chamber equipped with gloves by casting 20 μL of polymer solution onto the glass substrate placed in a glass vessel. With the volatilization of organic solvent, the transparent solution became turbid, and honeycomb films were obtained after complete solvent evaporation. The films were then dried in a 50 °C vacuum oven for 4 h for subsequent experiments. To investigate the photoreconfiguration of honeycomb films, we placed the samples on a leveling bench with adjustable slope angle. Typically, a vertical beam of 450 nm polarized light with intensity of 1000 mW/cm^2, which was generated by an LED lamp and a polaroid, was applied to induce the reconfiguration. After irradiation for a certain amount of time, the beam was shut off, and samples were collected for other characterizations. All of these experiments were carried out at room temperature under ambient conditions.

Fabrication of Etched Pattern on Silicon Wafer. The top layer of the honeycomb film before or after photoreconfiguration was transferred onto a silicon wafer substrate that had been spin-coated with an ethanol solution of poly(styrene-*co*-allyl alcohol) (4 wt %). The honeycomb film was placed with the original top surface (with pores) facing the sacrificial coating and subsequently oven-dried at 50 °C for 1 h. Next, the glass substrate and inverted bottom layer of the honeycomb film was peeled off, leaving the porous surface layer of the honeycomb film on the silicon wafer. A porous polymeric mask was thus formed on the silicon wafer. The silicon wafer with polymeric mask was then etched by CF_4-based inductively coupled plasma reactive ion etching (ICP-RIE). The remaining mask after etching was thoroughly removed by rinsing in chloroform. Eventually, a honeycomb pattern was transferred onto a silicon wafer.

Instruments and Measurements. The morphologies of the films were first observed with an optical microscope (Cryo-CSS450), and the images were taken with a digital camera. The elaborate morphologies of the films were obtained from SEM (S-4800, HITACHI) operated at an accelerating voltage of 15.0 kV after being coated by a thin layer of sputtered Au. AFM images were obtained with multimode atomic force microscopy (PARK/XE-100) using noncontact mode under ambient conditions. The LED lamp (Uvata UP114) with a wavelength of 450 nm was used as the light source for the photoreconfiguration experiments. Etching was performed by ICP-RIE (ICP-98A, Institute of Microelectronics of Chinese Academy of Sciences) with a CF_4 flow rate of 30 standard cubic centimeters per minute (sccm), a cavity pressure of 1.0 Pa, a source power density of ∼1.85 W/cm^2, and a bias power density of ∼0.53 W/cm^2. A self-bias of ∼160 V was developed in the etching cavity.

RESULTS AND DISCUSSION

Preparation of Large Area BFAs with Controllable Morphology. The morphology of BFAs relies on the nucleation and growth of water droplets, which are susceptible to experimental parameters, such as relative humidity, concentration, polymer type, and polymer composition. With an optimized static BF process, the uncertainties have been further minimized to tolerate various casting conditions and facilitate the formation of ordered BFAs on a large scale.[37−41]

A typical static BF process was performed as described in the Experimental Section. A droplet of 1 wt % CS_2 solution of P4VP$_{54}$-*b*-PAzoMA$_{112}$ (PVP$_{54}$AZ$_{112}$) copolymer was cast on a glass substrate under 80% relative humidity (RH) to prepare a BF film. The film was taken out after the solvent completely evaporated. An optical microscope image (Figure 1a) and an SEM image (Figure 1b and Figure S1) reveal that the preparation of monocrystalline honeycomb lattice in a millimeter area has been achieved by the simple static BF process. As expected, the film with highly ordered structure exhibits nacre color due to sunlight diffraction and interference effects (inset in Figure 1a). The fast Fourier transform (FFT) of the SEM image (inset in Figure S1), with first- and high-order spots, demonstrates highly ordered two-dimensional hexagonal arrangement of the pores. SEM (inset in Figure 1b) and AFM (Figure 1c) observations along the cross-sectional view indicate that uniform monolayer spherical pores with a diameter (d) of (1.80 ± 0.05) μm and pore-to-pore distance (D) of (2.10 ± 0.06) μm are formed.

The variation of polymer concentration affects both the evaporation rate and the convection of the solution, resulting in BFAs with different surface features. As shown in Figure 1b and d−f, the diameter of the pores decreases from (2.18 ± 0.04) μm to (1.38 ± 0.04) μm with decreasing polymer

DOI: 10.1021/acsami.6b14024
ACS Appl. Mater. Interfaces 2017, 9, 4223−4230

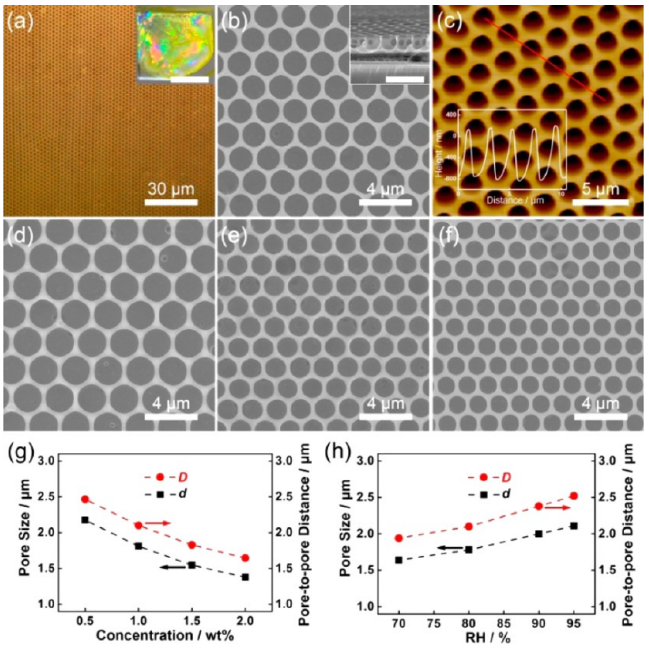

Figure 1. Morphological analysis of the honeycomb films prepared by the $PVP_{54}AZ_{112}$ copolymer. (a) Optical microscope image; (inset) digital camera photo; scale bar: 5 mm. (b) SEM image; (inset) cross-section view; scale bar: 4 μm. (c) AFM image. (d–f) SEM images of the honeycomb films fabricated at polymer concentrations of (d) 0.5, (e) 1.5, and (f) 2.0 wt %. (g,h) Morphological analysis of the honeycomb films prepared under variation of (g) polymer concentration and (h) RH.

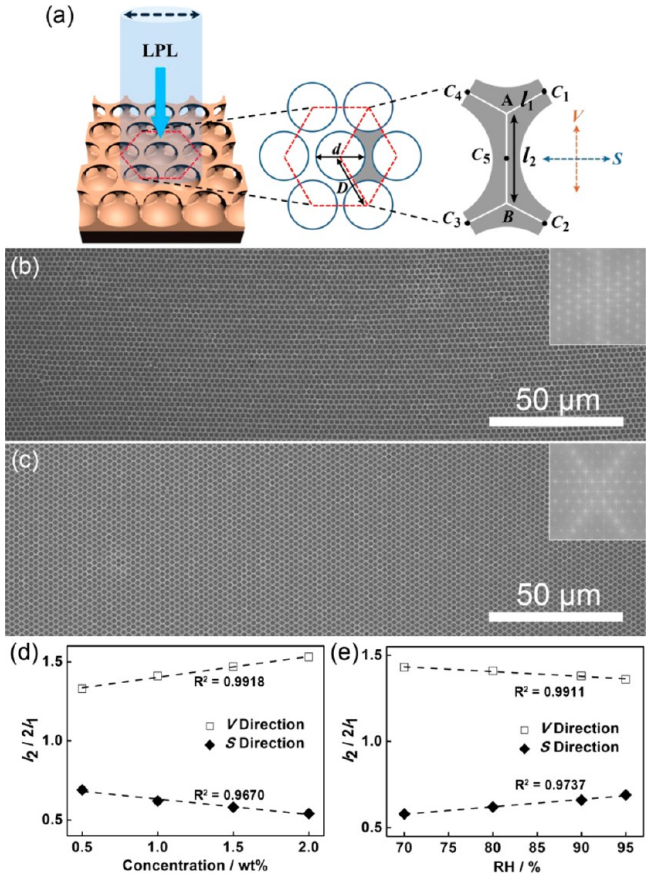

Figure 2. Scheme and SEM images of photoreconfiguration patterns for different light polarization and pristine films. (a) Deformation unit model of pristine SEM images and scheme of two types of irradiation. (b,c) Large-area reshaped pattern upon LPL irradiation in the (b) *V* direction (inset: FFT of the image) and (c) *S* direction (inset: FFT of the image). (d,e) Plotted analysis of photoreconfigured BFAs upon LPL irradiation for 30 min of various honeycomb films with different pristine morphologies upon variation of (d) concentration and (e) RH.

concentration from 0.5 to 2.0 wt %. The correlation between the pore size and polymer concentration is plotted in Figure 1g, which is consistent with our previous report.[42] The influence of RH on film morphology is shown in Figure 1h and Figure S2. With increasing atmospheric humidity from 70 to 95%, the growth rate of droplets becomes higher and leads to the pore sizes increasing from (1.44 ± 0.03) μm to (2.11 ± 0.07) μm. Therefore, a series of honeycomb films with controllable pore size have been prepared successfully by tuning solution concentration and RH during the breath figure process. It should be noted that the influences of polymer concentration and RH on the morphology are not identical in all BF systems. Because of the complexity of the BF process, the variation of solute, solvent, moist atmosphere, and other factors may produce a thoroughly conversed change trend.[43,44] In this BF system, adequate stabilizing capacity for water droplets of the amphiphilic copolymer, enough volatility of the CS_2 solvent, and a stable, moist atmosphere provided by the static BF method synergistically contribute to the formation of a typical pore size variation tendency along with the change of concentration and RH.[45]

Photoreconfiguration Behavior of the Honeycomb Films. Various BFAs fabricated from copolymer $PVP_{54}AZ_{112}$ under different conditions are adopted to investigate the influence of film morphology on photoreconfiguration of BFAs. To visualize and quantify the pore reshaping, we defined a unit cell as the rhombic area (one-third of the hexagonal lattice) based on the periodicity and symmetry of BFAs as schematically shown in Figure 2a. The magnified shadow part represents the deformation unit (DU), where the middle points of pores are denoted by capital letter C. Points A and B are the barycenter of the triangle-connected pores. For the pristine honeycomb films, the value of l_2 (the length between points A and B) is twice that of l_1 (the length between a middle point and its adjacent barycenter).

Because of the directionality of photofluidization and anisotropy of the BFAs, the relative direction between LPL polarization and BFA orientation would definitely influence the photoreconfiguration. Two characteristic polarization directions of the LPL, including the *V* direction (along the AB axis) and *S* direction (perpendicular to the AB axis), were chosen to carry out the photoreconfiguration. After being irradiated by vertical incident LPL for 30 min, morphologies of these reshaped films were observed by SEM as depicted in Figures S3 and S4. Large-area SEM images of reshaped BFAs are shown in Figure 2b and c. When the light polarization was along the *V* direction, the pores could be converted to a rectangular shape. While the polarization was in the *S* direction, the pores were molded into a rhombic shape. The corresponding FFT of the SEM images (insets in Figure 2b and c) indicated that the reshaped structures are also of high regularity and maintain two-dimensional hexagonal symmetry.

Upon vertical incident irradiation LPL, the azobenzene units in *trans* state reoriented orthogonally to the polarization direction. The whole copolymer chain was subsequently

DOI: 10.1021/acsami.6b14024
ACS Appl. Mater. Interfaces 2017, 9, 4223–4230

Table 1. Analysis of Film Morphologies Prepared by Copolymers $PVP_{54}AZ_{112}$ Fabricated at Various Concentrations and RH

	various concn under RH of 80%				various RH at concn of 1 wt %		
condition	0.5 wt %	1 wt %	1.5 wt %	2 wt %	70%	90%	95%
f	0.30	0.33	0.35	0.36	0.34	0.35	0.35
f/D	0.12	0.16	0.19	0.22	0.18	0.15	0.14

actuated by the photoalignment of the azobenzene units and thus resulted in directional mass migration.[46] In addition, because of high optical absorption efficiency of the azobenzene units, the incident LPL light was mostly absorbed by the surface of the photoresponsive architecture, and therefore, the directional photofluidization tended to occur preferably at the surface layer of BFAs.[47,48] Consequently, the actual action of photofluidization manifested as the expansion and elongation along the direction parallel to the light polarization in the horizontal plane and was accompanied by contraction against the polarization direction due to the isovolumetric effect.[27] The degree of photoinduced pore reshaping under various fabrication conditions can be quantified by the ratio of $l_2/2l_1$ plotted in Figure 2d and e. In the case of V direction irradiation, the sides of DU tended to stretch along the AB direction due to the directional photofluidization, which led to the increase of l_2 and decrease of l_1 ($l_2/2l_1 > 1$). In contrast, when the light polarization was along the S direction, the sides of DU tended to shrink along the AB direction, which resulted in a decrease of l_2 and increase of l_1 ($l_2/2l_1 < 1$). Although all the films were made of homogeneous copolymer, distinct $l_2/2l_1$ values were measured after the photoreconfiguration. As shown in Figure 2d, with the increasing polymer concentration, the resulting reshaping degree is also increased. Additionally, slight pore reshaping has been observed when the RH value increases (see Figure 2e). In both cases, the values of $l_2/2l_1$ reveal a reasonable relationship with corresponding polymer concentration or RH values. The linear correlation is described by eq 1, where l_0 denotes the intercept, K_{de} denotes the slope, and $[Co]$ represents the value of the polymer concentration or RH. The fitting parameters for Figure 2d and e are shown in Table S3.

$$l_2/2l_1 = l_0 + K_{de}[Co] \quad (1)$$

As shown in Figure 2a, the reshaping of DU is thoroughly derived from the photoreconfiguration of polymeric walls, and the pore region does not contribute to the photomanipulation process. Consequently, the unit cell composed of a large polymeric DU area and small pore size might be reshaped more obviously by the LPL treatment, i.e., photoreconfiguration degrees (De) is positively correlated with the surface area fraction of the polymer (f, eq 2). According to our recent study, the photoreconfiguration degree of aggregates formed by identical azobenzene-containing copolymers decreased with the increase of aggregate size under identical LPL irradiation.[49] For a unit cell of BFAs, the aggregate size can be represented by D. Therefore, the tendency of De should be positively correlated with f/D. Here, the values of f and f/D were calculated and listed in Table 1. The linear relationship between $l_2/2l_1$ and f/D are plotted in Figure S5 and represented as eq 3, which indicates the De value increases linearly with the value f/D. The fitting parameters for Figure S5 are listed in Table S4. The establishment of eq 3 allows us to predict pore reshaping in films fabricated by the same azobenzene-containing polymer.

$$f = 1 - \frac{\pi d^2}{2\sqrt{3}D^2} \quad (2)$$

$$l_2/2l_1 = l_0 + K_{de}(f/D) \quad (3)$$

The P4VP-*b*-PAzoMA copolymers adopted in this study are listed in Table S1. According to the SEM images shown in Figure 3a, d, g, and j, all of these polymers successfully form

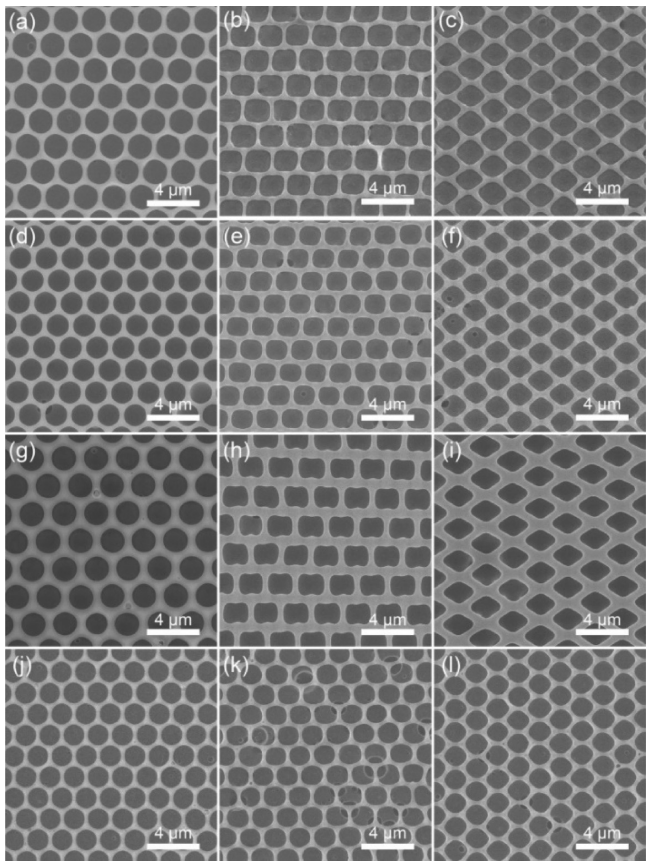

Figure 3. Pristine and reshaped BFAs upon LPL irradiation for 30 min prepared by different P4VP-*b*-PAzoMA copolymers. Images in the left, middle, and right columns are round pores, irradiated by LPL in the V direction, and irradiated by LPL in the S direction, respectively: (a–c) $PVP_{54}AZ_{112}$, (d–f) $PVP_{69}AZ_{74}$, (g–i) $PVP_{50}AZ_{51}$, and (j–l) $PVP_{69}AZ_{30}$.

honeycomb films with hexagonally arranged round pores. The detailed morphological analysis of these honeycomb films is shown in Table S5. Upon vertical incident LPL irradiation for 30 min, all of the films have been obviously reshaped (see Figure 3). In addition, the photoinduced reshaping degree was observed to be highly dependent on the contents of azobenzene moieties in the polymer (see Table S5). Despite the decrease of the f/D value, larger reshaping degrees were observed on the films fabricated by $PVP_{54}AZ_{112}$ than those of $PVP_{69}AZ_{74}$ and $PVP_{69}AZ_{30}$. This positive relationship with the contents of the PAzoMA block is in accordance with our

DOI: 10.1021/acsami.6b14024
ACS Appl. Mater. Interfaces 2017, 9, 4223–4230

previous result.[35,36] The most distinct reshaping was observed on the honeycomb films fabricated by copolymer $PVP_{50}AZ_{51}$ due to the large *f/D* value and relatively high azobenzene content, resulting inunique dumbbell-shaped pores upon LPL irradiation along the *V* direction.

For the versatility of directional photomanipulation of BFAs to be further verified, various azobenzene-containing polymers, as listed in Table S2, were adopted to prepare honeycomb films. As shown in Figure 4a–c, round pores in the PMMAzo homopolymer BF film could be reshaped into rhombic and rectangular pores with thick polymeric walls. Round pores in the diblock copolymer PDMS-*b*-PAzoMA BF film were converted into an elliptical shape (Figure 4d–f). In Figure 4g–i, pores with small opening fabricated from triblock copolymer PEO-*b*-PS-*b*-$(PMMAzo)_2$ were transformed into long slits with a width of (200 ± 40) nm and length of around (1.00 ± 0.11) μm. Therefore, directional photomanipulation is suitable for a variety of azobenzene-containing homo- and copolymers, which provides a platform for the preparation of films with different reshaped micropatterns.

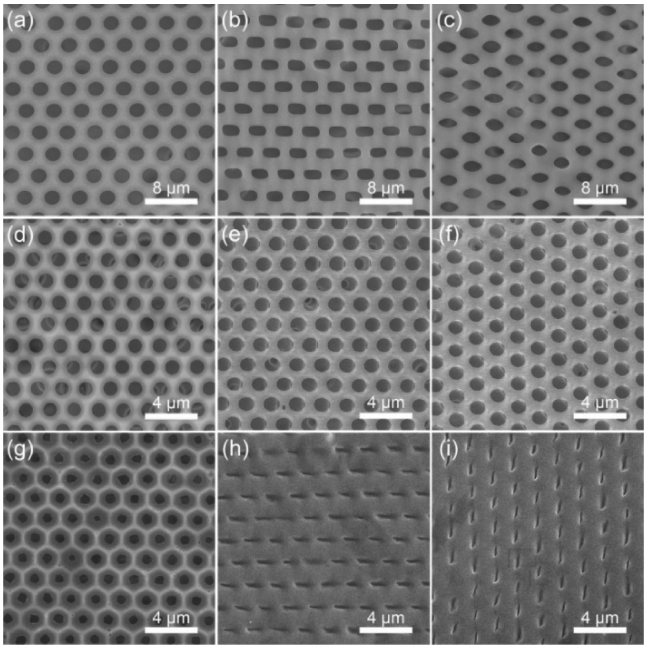

Figure 4. Pristine and reshaped BFAs upon LPL irradiation for 30 min prepared by different azobenzene-containing copolymers. Images in the left, middle, and right columns are round pores, irradiated by LPL in the *V* direction, and irradiated by LPL in the *S* direction, respectively: (a–c) PMMAzo homopolymer, (d–f) PDMS-*b*-PAzoMA diblock copolymer, and (g–i) PEO-*b*-PS-*b*-$(PMMAzo)_2$ triblock copolymer.

In addition to the vertical incident LPL, oblique incidence LPL was also applied to investigate the photoreconfiguration effect on the honeycomb patterns. Typically, the slant angle was set at 45°, and the LPL was polarized perpendicular to the incident direction in the slant plane as illustrated in Figure 5a. According to the SEM images shown in Figure 5b and c, round-rectangle or round-rhombic pores were obtained under the LPL irradiation along the *V* or *S* direction, respectively, for 30 min. The two perpendicular cross-section views of the BF film in Figure 5b showed unique asymmetrical structures inside the pores in Figure 5d and e, which was different than the symmetric architecture upon vertical-incident LPL irradiation.[27]

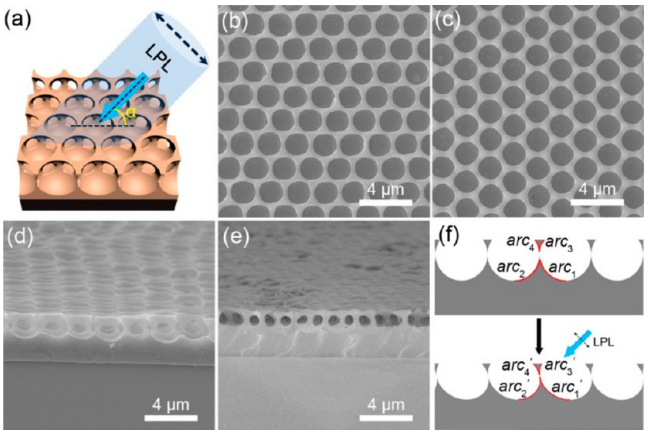

Figure 5. (a) Scheme of slantwise LPL irradiation. (b–e) SEM images of reshaped pores upon 45° slanted LPL irradiation for 30 min: (b) round-rectangle pores, (c) round-rhombic pores, (d) longitudinal cross-section SEM view of (b), (e) lateral cross-section SEM view of (b). (f) Scheme of asymmetry deformation in the pores.

Herein, slantwise irradiation could be divided into two parts. The vertical part only contributed to the photoreshaping as mentioned and reported previously. The horizontal part resulted in the inner asymmetrical structure. As illustrated in Figure 5f, under LPL irradiation with a slant angle of 45°, the walls parallel to the light polarization (arc_1 and arc_4) would expand and stretch along the polarization direction to form elongated walls labeled as arc_1' and arc_4'. Their opposite walls (arc_2 and arc_3) trended to contraction against the polarization direction to form the contracted walls of arc_2' and arc_3'. On the other hand, the walls perpendicular to the irradiation plane would not be influenced by the slant direction of irradiation and remain symmetrical. Accordingly, the inner asymmetrical structures could be created by directional photomanipulation under slantwise LPL irradiation.

Different than LPL, CPL does not feature a linear polarization direction due to the clockwise rotating electric field vector.[50−53] Under vertical incident CPL irradiation, such as the left-handed CPL illustrated in Figure 6a, round pores

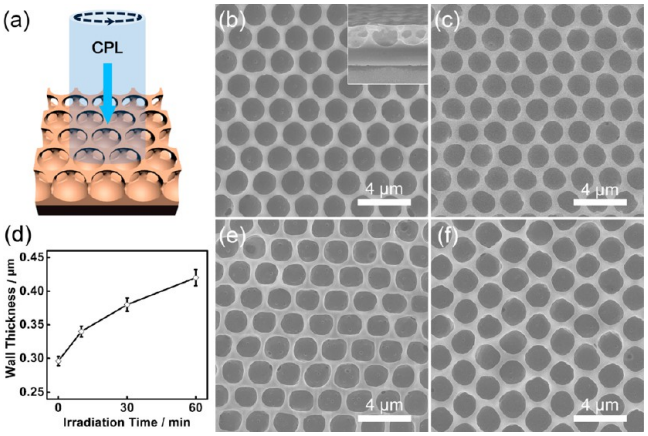

Figure 6. (a) Scheme of CPL irradiation. (b,c) SEM images of reshaped pores upon CPL irradiation for (b) 30 min (inset: cross-section view) and (c) 60 min. (d) Relationship between average wall thickness and CPL irradiation time. (e,f) SEM images of honeycomb films after a secondary photomanipulation: (e) rectangle and (f) rhombic pores.

DOI: 10.1021/acsami.6b14024
ACS Appl. Mater. Interfaces 2017, 9, 4223−4230

were reshaped in an isotropic manner on the horizontal plane. As shown in Figure 6b and c, the round shape of pores was maintained during the entire photoreconfiguration process. The inset in Figure 6b shows that the rotational symmetry of the porous structures was almost preserved and that the depth of the pores was visibly reduced after photoreconfiguration for 30 min. In addition, an obvious increase of the wall thickness with a slight increase of polydespersity was observed from (0.30 ± 0.01) μm to (0.42 ± 0.02) μm upon CPL irradiation for 1 h as plotted in Figure 6d. Herein, the rotating electric field vector of the CPL features isotropic polarization in all in-plane directions.[54,55] Therefore, CPL gave rise to uniform photofluidization to the azobenzene-containing copolymer walls toward the radial direction and resulted in isotropic expansion of the walls in the horizontal plane.[56] Consequently, CPL irradiation enlarged the polymeric wall thickness while maintaining the pristine pore shape, which allows a facile manipulation of wall thickness upon both pristine and reshaped BFAs. For instance, the walls of rectangle (Figure S3b) and rhombic pores (Figure S3f) obtained by vertical incident LPL irradiation could be further swelled by CPL irradiation as shown in Figure 6e and f.

BFA Etching Mask and Pattern Transfer. The facile and flexible photomanipulation method affords predictable and deterministic manipulation of the shape and size of pores on BFAs by a noncontact manner for a number of promising applications.[20−22] Following the process depicted in Figure 7a, the surface layers of the BF films were peeled off before and after photoreconfiguration and subsequently served as an etching mask with tunable pore shapes. The SEM images of inverted surface layers with round, rectangular, and rhombic pores transferred onto a silicon wafer are shown in Figure 7b−d, respectively. The inset of Figure 7b reveals the magnified topography of round pores on the inverted surface layer. Upon CF_4 etching for 10 min, definite porous structures were transferred on the surface of silicon wafers after thoroughly washing off the residual polymeric mask.[57−59] As shown in Figure 7e−g, the obtained patterns were highly similar to their corresponding polymeric masks. The AFM height images in Figure 7h−j confirm that the depth of these honeycomb porous structures on silicon wafers is around 300 nm. These hexagonally arranged pores embedded on the silicon wafer surface show great feasibility for preparing anisotropic hydrophobic surfaces and an elaborate microreactor.[52,60,61] Furthermore, the photoinduced reshaping of pores can also be conducted after transferring the surface layer onto the silicon wafer (see Scheme S1 and Figure S6), which provides readily phototunable masks to adapt the requirements of different etching applications.

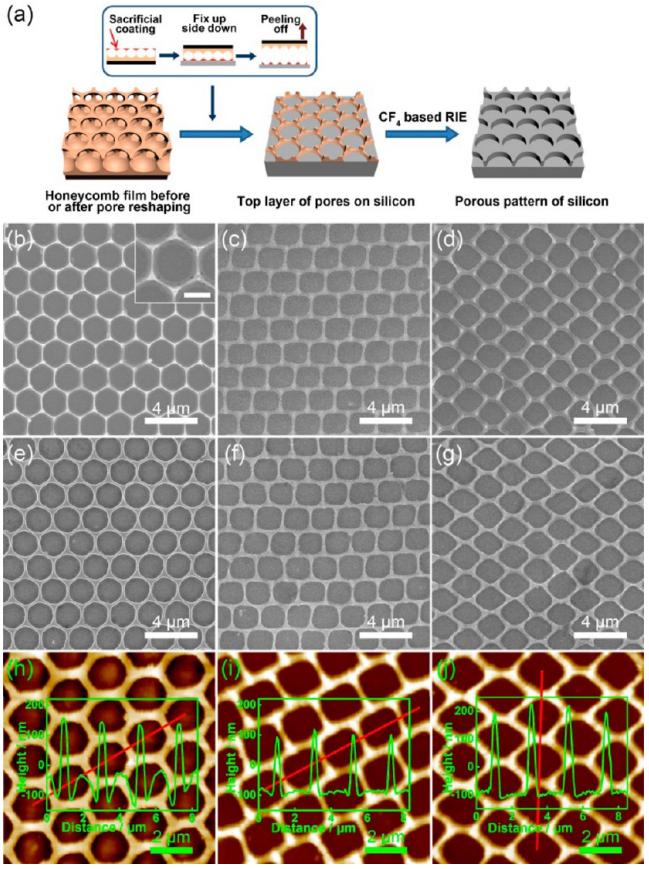

Figure 7. (a) Scheme of the pattern transfer process from a honeycomb film to silicon wafer. (b−d) SEM images of inverted top layers on silicon with (b) round (inset: magnified view; scale bar: 1 μm), (c) rectangular, and (d) rhombic pores. (e−g) SEM images of patterned silicon with (e) round, (f) rectangular, and (g) rhombic pores. (h−j) AFM measurements of porous pattern of the silicon wafer with (h) round, (i) rectangular, and (j) rhombic pores.

CONCLUSIONS

In summary, a comprehensive investigation of the photomanipulation of large-area BFAs confirmed that directional photomanipulation could serve as a powerful way to manipulate the as-prepared microstructures in a noncontact and nondestructive manner. Upon polarized beam irradiation, deterministic and predictable photoreconfiguration of BFAs has been achieved by simply tuning the initial morphology of the films, irradiation factors, and azobenzene-containing polymers. The technique is highly compatible with large-area, high-throughput fabrication processes and therefore provides a platform for preparing porous films with different micropatterns. Furthermore, it also shows exciting potential for applications of lithography, separation, photonic band gap, microelectronics, and so forth.

ASSOCIATED CONTENT

Supporting Information

The Supporting Information is available free of charge on the ACS Publications website at DOI: 10.1021/acsami.6b14024.

Characteristics of azobenzene-containing polymers, SEM images of BF films fabricated under various conditions, SEM images of reshaped BFAs fabricated under various conditions, correlation analysis between the value of $l_2/2l_1$ and fabrication condition, correlation analysis between the value of $l_2/2l_1$ and the value of f/D, morphological analysis of pristine and reshaped films prepared by various copolymers, pattern transfer process illustration, and SEM images of a readily phototunable etching mask and corresponding patterned silicon (PDF)

AUTHOR INFORMATION

Corresponding Authors

*E-mail: jlin@ecust.edu.cn (J.L.).
*E-mail: lilei@xmu.edu.cn (L.L.).
*E-mail: slin@ecust.edu.cn (S.L.).

DOI: 10.1021/acsami.6b14024
ACS Appl. Mater. Interfaces 2017, 9, 4223−4230

ORCID
Jiaping Lin: 0000-0001-9633-4483
Lei Li: 0000-0003-2732-9116

Notes

The authors declare no competing financial interest.

■ ACKNOWLEDGMENTS

This work was supported by National Natural Science Foundation of China (51622301, 51573046, 51573088, 51373143, and 21674087) and the Natural Science Foundation of Fujian Province (No. 2014J0105). Support from Projects of Shanghai Municipality (14SG29) and Fundamental Research Funds for the Central Universities (B14018 and WD1213002) is also appreciated.

■ REFERENCES

(1) Liu, Q. Q.; Tang, Z.; Ou, B. L.; Liu, L. H.; Zhou, Z. H.; Shen, S. H.; Duan, Y. X. Design, Preparation, and Application of Ordered Porous Polymer Materials. *Mater. Chem. Phys.* **2014**, *144*, 213−225.
(2) Wan, L.-S.; Li, J.-W.; Ke, B.-B.; Xu, Z.-K. Ordered Microporous Membranes Templated by Breath Figures for Size-Selective Separation. *J. Am. Chem. Soc.* **2012**, *134*, 95−98.
(3) Zhu, Y.; Sheng, R.; Luo, T.; Li, H.; Sun, J.; Chen, S.; Sun, W.; Cao, A. Honeycomb-Structured Films by Multifunctional Amphiphilic Biodegradable Copolymers: Surface Morphology Control and Biomedical Application as Scaffolds for Cell Growth. *ACS Appl. Mater. Interfaces* **2011**, *3*, 2487−2495.
(4) Billon, L.; Manguian, M.; Pellerin, V.; Joubert, M.; Eterradossi, O.; Garay, H. Tailoring Highly Ordered Honeycomb Films Based on Ionomer Macromolecules by the Bottom-Up Approach. *Macromolecules* **2009**, *42*, 345−356.
(5) Zhou, W.; Chen, J.; Li, Y.; Wang, D.; Chen, J.; Feng, X.; Huang, Z.; Liu, R.; Lin, X.; Zhang, H.; Mi, B.; Ma, Y. Copper Mesh Templated by Breath-Figure Polymer Films as Flexible Transparent Electrodes for Organic Photovoltaic Devices. *ACS Appl. Mater. Interfaces* **2016**, *8*, 11122−11127.
(6) Li, L.; Zhong, Y. W.; Li, J.; Gong, J. L.; Ben, Y.; Xu, J.; Chen, X. P.; Ma, Z. Breath Figure Lithography: A Facile and Versatile Method for Micropatterning. *J. Colloid Interface Sci.* **2010**, *342*, 192−197.
(7) Han, W.; Li, B.; Lin, Z. Drying-Mediated Assembly of Colloidal Nanoparticles into Large-Scale Microchannels. *ACS Nano* **2013**, *7*, 6079−6085.
(8) Byun, M.; Han, W.; Li, B.; Xin, X.; Lin, Z. An Unconventional Route to Hierarchically Ordered Block Copolymers on a Gradient Patterned Surface through Controlled Evaporative Self-Assembly. *Angew. Chem., Int. Ed.* **2013**, *52*, 1122−1127.
(9) Han, W.; He, M.; Byun, M.; Li, B.; Lin, Z. Large-Scale Hierarchically Structured Conjugated Polymer Assemblies with Enhanced Electrical Conductivity. *Angew. Chem., Int. Ed.* **2013**, *52*, 2564−2568.
(10) Li, B.; Han, W.; Jiang, B.; Lin, Z. Crafting Threads of Diblock Copolymer Micelles via Flow-Enabled Self-Assembly. *ACS Nano* **2014**, *8*, 2936−2942.
(11) Li, B.; Zhang, C.; Jiang, B.; Han, W.; Lin, Z. Flow-Enabled Self-Assembly of Large-Scale Aligned Nanowires. *Angew. Chem., Int. Ed.* **2015**, *54*, 4250−4254.
(12) Ma, H. M.; Hao, J. C. Ordered Patterns and Structures via Interfacial Self-assembly: Superlattices, Honeycomb Structures and Coffee Rings. *Chem. Soc. Rev.* **2011**, *40*, 5457−5471.
(13) Munoz-Bonilla, A.; Fernandez-Garcia, M.; Rodriguez-Hernandez, J. Towards Hierarchically Ordered Functional Porous Polymeric Surfaces Prepared by the Breath Figures Approach. *Prog. Polym. Sci.* **2014**, *39*, 510−554.
(14) Zhang, A.; Bai, H.; Li, L. Breath Figure: A Nature-Inspired Preparation Method for Ordered Porous Films. *Chem. Rev.* **2015**, *115*, 9801−9868.
(15) Bai, H.; Du, C.; Zhang, A. J.; Li, L. Breath Figure Arrays: Unconventional Fabrications, Functionalizations, and Applications. *Angew. Chem., Int. Ed.* **2013**, *52*, 12240−12255.
(16) Wan, L. S.; Zhu, L. W.; Ou, Y.; Xu, Z. K. Multiple Interfaces in Self-Assembled Breath Figures. *Chem. Commun.* **2014**, *50*, 4024−4039.
(17) Bui, V.-T.; Ko, S. H.; Choi, H.-S. Large-Scale Fabrication of Commercially Available, Nonpolar Linear Polymer Film with a Highly Ordered Honeycomb Pattern. *ACS Appl. Mater. Interfaces* **2015**, *7*, 10541−10547.
(18) Martínez-Campos, E.; Elzein, T.; Bejjani, A.; García-Granda, M. J.; Santos-Coquillat, A.; Ramos, V.; Muñoz-Bonilla, A.; Rodríguez-Hernández, J. Toward Cell Selective Surfaces: Cell Adhesion and Proliferation on Breath Figures with Antifouling Surface Chemistry. *ACS Appl. Mater. Interfaces* **2016**, *8*, 6344−6353.
(19) Beattie, D.; Wong, K. H.; Williams, C.; Poole-Warren, L. A.; Davis, T. P.; Barner-Kowollik, C.; Stenzel, M. H. Honeycomb-Structured Porous Films from Polypyrrole-Containing Block Copolymers Prepared via RAFT Polymerization as a Scaffold for Cell Growth. *Biomacromolecules* **2006**, *7*, 1072−1082.
(20) Lee, J.; Jeong, Y.-C.; Kim, Y.; Choi, J.; Park, J.-K. Optically Tunable and Reconfigurable Azobenzene Photonic Crystal. *Macromol. Res.* **2014**, *22*, 606−612.
(21) Phillips, K. R.; Vogel, N.; Hu, Y.; Kolle, M.; Perry, C. C.; Aizenberg, J. Tunable Anisotropy in Inverse Opals and Emerging Optical Properties. *Chem. Mater.* **2014**, *26*, 1622−1628.
(22) Choi, D.-H; Yoon, G.-W.; Park, J. W.; Ihm, C.; Lee, D.-S.; Yoon, J.-B. Fabrication of a Membrane Filter with Controlled Pore Shape and its Application to Cell Separation and Strong Single Cell Trapping. *J. Micromech. Microeng.* **2015**, *25*, 105007.
(23) Li, J.; Peng, J.; Huang, W.; Wu, Y.; Fu, J.; Cong, Y.; Xue, L.; Han, Y. Ordered Honeycomb-Structured Gold Nanoparticle Films with Changeable Pore Morphology: From Circle to Ellipse. *Langmuir* **2005**, *21*, 2017−2021.
(24) Nishikawa, T.; Nonomura, M.; Arai, K.; Hayashi, J.; Sawadaishi, T.; Nishiura, Y.; Hara, M.; Shimomura, M. Micropatterns Based on Deformation of a Viscoelastic Honeycomb Mesh. *Langmuir* **2003**, *19*, 6193−6201.
(25) Yabu, H.; Jia, R.; Matsuo, Y.; Ijiro, K.; Yamamoto, S.-a.; Nishino, F.; Takaki, T.; Kuwahara, M.; Shimomura, M. Preparation of Highly Oriented Nano-Pit Arrays by Thermal Shrinking of Honeycomb-Patterned Polymer Films. *Adv. Mater.* **2008**, *20*, 4200−4204.
(26) Jia Ruokun, L. T.; Zhou, S. Shrinking and Light Diffraction of the Self-Organized Polystyrene-*block*-Polybutadiene Microporous Film Deposited on a Stretched Polymer Film by Thermal Contraction. *Chin. J. Appl. Chem.* **2014**, *31*, 560−565.
(27) Wang, W.; Du, C.; Wang, X.; He, X.; Lin, J.; Li, L.; Lin, S. Directional Photomanipulation of Breath Figure Arrays. *Angew. Chem., Int. Ed.* **2014**, *53*, 12116−12119.
(28) Lee, S.; Kang, H. S.; Park, J.-K. Directional Photofluidization Lithography: Micro/Nanostructural Evolution by Photofluidic Motions of Azobenzene Materials. *Adv. Mater.* **2012**, *24*, 2069−2103.
(29) Wang, Y.; Lin, S.; Zang, M.; Xing, Y.; He, X.; Lin, J.; Chen, T. Self-Assembly and Photo-Responsive Behavior of Novel ABC_2-type Block Copolymers Containing Azobenzene Moieties. *Soft Matter* **2012**, *8*, 3131−3138.
(30) Priimagi, A.; Shevchenko, A. Azopolymer-based Micro- and Nanopatterning for Photonic Applications. *J. Polym. Sci., Part B: Polym. Phys.* **2014**, *52*, 163−182.
(31) Zhou, X.; Du, Y.; Wang, X. Azo Polymer Microspheres with Photo-Manipulated Surface and Topographic Structure. *Macromol. Chem. Phys.* **2016**, *217*, 765−772.
(32) Yu, H.; Kobayashi, T. Photoresponsive Block Copolymers Containing Azobenzenes and Other Chromophores. *Molecules* **2010**, *15*, 570−603.
(33) Yu, H. Photoresponsive Liquid Crystalline Block Copolymers: From Photonics to Nanotechnology. *Prog. Polym. Sci.* **2014**, *39*, 781−815.

DOI: 10.1021/acsami.6b14024
ACS Appl. Mater. Interfaces 2017, 9, 4223−4230

(34) Pirani, F.; Angelini, A.; Frascella, F.; Rizzo, R.; Ricciardi, S.; Descrovi, E. Light-Driven Reversible Shaping of Individual Azopolymeric Micro-Pillars. *Sci. Rep.* **2016**, *6*, 31702.
(35) Lin, S.; Wang, Y.; Cai, C.; Xing, Y.; Lin, J.; Chen, T.; He, X. Tuning Self-Assembly and Photo-Responsive Behavior of Azobenzene-Containing Triblock Copolymers by Combining Homopolymers. *Nanotechnology* **2013**, *24*, 085602.
(36) Wang, W.; Lin, J.; Cai, C.; Lin, S. Optical Properties of Amphiphilic Copolymer-based Self-Assemblies. *Eur. Polym. J.* **2015**, *65*, 112−131.
(37) De León, A. S.; Garnier, T.; Jierry, L.; Boulmedais, F.; Muñoz-Bonilla, A.; Rodríguez-Hernández, J. Enzymatic Catalysis combining the Breath Figures and Layer-by-Layer Techniques: Toward the Design of Microreactors. *ACS Appl. Mater. Interfaces* **2015**, *7*, 12210−12219.
(38) Zhu, L. W.; Wu, B. H.; Wan, L. S.; Xu, Z.-K. Polystyrene with Hydrophobic End Groups: Synthesis, Kinetics, Interfacial Activity, and Self-Assemblies Templated by Breath Figures. *Polym. Chem.* **2014**, *5*, 4311−4320.
(39) Li, X.; Zhao, Q.; Xu, T.; Huang, J.; Wei, L.; Ma, Z. Highly Ordered Microporous Polystyrene-*b*-Poly(acrylic acid) Films: Study on the Influencing Factors in Their Fabrication via a Static Breath-Figure Method. *Eur. Polym. J.* **2014**, *50*, 135−141.
(40) Lv, C.; Cui, K.; Li, S.; Wu, H.; Ma, Z. Polystyrene-*b*-Poly(2,2,2-trifluoroethyl acrylate)-*b*-Polystyrene Copolymers: Synthesis and Fabrication of their Hydrophobic Porous Films, Spheres, and Fibers. *J. Polym. Sci., Part A: Polym. Chem.* **2016**, *54*, 678−685.
(41) Ding, L.; Zhang, A.; Li, W.; Bai, H.; Li, L. Multi-Length Scale Porous Polymer Films from Hypercrosslinked Breath Figure Arrays. *J. Colloid Interface Sci.* **2016**, *461*, 179−184.
(42) Gao, F.; Wang, W.; Li, X.; Li, L.; Lin, J.; Lin, S. Fabrication of Ordered Honeycomb Amphiphobic Films with Extremely Low Fluorine Content. *J. Colloid Interface Sci.* **2016**, *468*, 70−77.
(43) Du, M.; Zhu, P.; Yan, X.; Su, Y.; Song, W.; Li, J. Honeycomb Self-Assembled Peptide Scaffolds by the Breath Figure Method. *Chem. - Eur. J.* **2011**, *17*, 4238−4245.
(44) Li, H.; Jia, Y.; Du, M.; Fei, J.; Zhao, J.; Cui, Y.; Li, J. Self-Organization of Honeycomb-like Porous TiO2 Films by means of the Breath-Figure Method for Surface Modification of Titanium Implants. *Chem. - Eur. J.* **2013**, *19*, 5306−5313.
(45) Hernandez-Guerrero, M.; Stenzel, M. H. Honeycomb Structured Polymer Films via Breath Figures. *Polym. Chem.* **2012**, *3*, 563−577.
(46) Yu, H.; Kobayashi, T. *Azobenzene-Containing Materials for Hologram*. Holograms - Recording Materials and Applications; InTech: Rijeka, 2011; Vol. *5*, p 95.
(47) Kang, H. S.; Lee, S.; Lee, S.-A.; Park, J.-K. Multi-Level Micro/Nanotexturing by Three-Dimensionally Controlled Photofluidization and its Use in Plasmonic Applications. *Adv. Mater.* **2013**, *25*, 5490−5497.
(48) Lee, S.-A.; Kang, H. S.; Park, J.-K.; Lee, S. Vertically Oriented, Three-Dimensionally Tapered Deep-Subwavelength Metallic Nanohole Arrays Developed by Photofluidization Lithography. *Adv. Mater.* **2014**, *26*, 7521−7528.
(49) Li, J.; Chen, L.; Xu, J.; Wang, K.; Wang, X.; He, X.; Dong, H.; Lin, S.; Zhu, J. Photoguided Shape Deformation of Azobenzene-Containing Polymer Microparticles. *Langmuir* **2015**, *31*, 13094−13100.
(50) Lee, S.; Shin, J.; Lee, Y.-H.; Park, J.-K. Fabrication of the Funnel-Shaped Three-Dimensional Plasmonic Tip Arrays by Directional Photofluidization Lithography. *ACS Nano* **2010**, *4*, 7175−7184.
(51) Lee, S.; Kang, H. S.; Park, J.-K. High-Resolution Patterning of Various Large-Area, Highly Ordered Structural Motifs by Directional Photofluidization Lithography: Sub-30-nm Line, Ellipsoid, Rectangle, and Circle Arrays. *Adv. Funct. Mater.* **2011**, *21*, 1770−1778.
(52) Lee, S.; Kang, H. S.; Ambrosio, A.; Park, J.-K.; Marrucci, L. Directional Superficial Photofluidization for Deterministic Shaping of Complex 3D Architectures. *ACS Appl. Mater. Interfaces* **2015**, *7*, 8209−8217.
(53) Rianna, C.; Calabuig, A.; Ventre, M.; Cavalli, S.; Pagliarulo, V.; Grilli, S.; Ferraro, P.; Netti, P. A. Reversible Holographic Patterns on Azopolymers for Guiding Cell Adhesion and Orientation. *ACS Appl. Mater. Interfaces* **2015**, *7*, 16984−16991.
(54) Liu, J.; Wang, M.; Dong, M.; Gao, L.; Tian, J. Distinguishing the Parallel and Vertical Orientations and Optic Axis Characteristics Determination of Azobenzene Mesogen by Conoscopic Polarized Microscopy. *J. Microsc.* **2011**, *244*, 144−151.
(55) Bin, J.; Oates, W. S. A Unified Material Description for Light Induced Deformation in Azobenzene Polymers. *Sci. Rep.* **2015**, *5*, 14654.
(56) Kang, H. S.; Lee, S.; Choi, J.; Lee, H.; Park, J.-K.; Kim, H.-T. Light-Induced Surface Patterning of Silica. *ACS Nano* **2015**, *9*, 9837−9848.
(57) Hirai, Y.; Yabu, H.; Matsuo, Y.; Ijiro, K.; Shimomura, M. Biomimetic Bi-Functional Silicon Nanospike-Array Structures Prepared by Using Self-Organized Honeycomb Templates and Reactive Ion Etching. *J. Mater. Chem.* **2010**, *20*, 10804−10808.
(58) Saito, Y.; Kawano, T.; Shimomura, M.; Yabu, H. Fabrication of Mussel-Inspired Highly Adhesive Honeycomb Films Containing Catechol Groups and Their Applications for Substrate-Independent Porous Templates. *Macromol. Rapid Commun.* **2013**, *34*, 630−634.
(59) Katiyar, A. K.; Mukherjee, S.; Zeeshan, M.; Ray, S. K.; Raychaudhuri, A. K. Enhancement of Efficiency of a Solar Cell Fabricated on Black Si Made by Inductively Coupled Plasma−Reactive Ion Etching Process: A Case Study of a n-CdS/p-Si Heterojunction Cell. *ACS Appl. Mater. Interfaces* **2015**, *7*, 23445−23453.
(60) Li, X.; Zhang, L.; Wang, Y.; Yang, X.; Zhao, N.; Zhang, X.; Xu, J. A Bottom-Up Approach to Fabricate Patterned Surfaces with Asymmetrical TiO_2 Microparticles Trapped in the Holes of Honeycomblike Polymer Film. *J. Am. Chem. Soc.* **2011**, *133*, 3736−3739.
(61) Wiktor, P.; Brunner, A.; Kahn, P.; Qiu, J.; Magee, M.; Bian, X.; Karthikeyan, K.; LaBaer, J. Microreactor Array Device. *Sci. Rep.* **2015**, *5*, 8736.

DOI: 10.1021/acsami.6b14024
ACS Appl. Mater. Interfaces 2017, 9, 4223−4230